USAARL Report 94-42

A Correlative Investigation of Simulated Occupant Motion and Accident Report in a Helicopter Crash

By

David G. Beale

Nabih M. Alem

Barclay P. Butler

Aircrew Protection Division

August 1994

United States Army Aeromedical Research Laboratory
Fort Rucker, Alabama 36362-0577

Notice

Qualified requesters

Qualified requesters may obtain copies from the Defense Technical Information Center (DTIC), Cameron Station, Alexandria, Virginia 22314. Orders will be expedited if placed through the librarian or other person designated to request documents from DTIC.

Change of address

Organizations receiving reports from the U.S. Army Aeromedical Research Laboratory on automatic mailing lists should confirm correct address when corresponding about laboratory reports.

Disposition

Destroy this document when it is no longer needed. Do not return it to the originator.

Disclaimer

The views, opinions, and/or findings contained in this report are those of the author(s) and should not be construed as an official Department of the Army position, policy, or decision, unless so designated by other official documentation. Citation of trade names in this report does not constitute an official Department of the Army endorsement or approval of the use of such commercial items.

Reviewed:

Kevin T. Mason

KEVIN T. MASON
LTC, MC, MFS
Director, Aircrew Protection Division

Released for publication:

Dennis F. Shanahan

DENNIS F. SHANAHAN
Colonel, MC, MFS
Commanding

Roger W. Wiley

ROGER W. WILEY, O.D., Ph.D.
Chairman, Scientific Review Committee

REPORT DOCUMENTATION PAGE

Form Approved
OMB No. 0704-0188

1a. REPORT SECURITY CLASSIFICATION Unclassified	1b. RESTRICTIVE MARKINGS
2a. SECURITY CLASSIFICATION AUTHORITY	3. DISTRIBUTION/AVAILABILITY OF REPORT Approved for public release, distribution unlimited
2b. DECLASSIFICATION/DOWNGRADING SCHEDULE	
4. PERFORMING ORGANIZATION REPORT NUMBER(S) USAARL Report No. 94-42	5. MONITORING ORGANIZATION REPORT NUMBER(S)
6a. NAME OF PERFORMING ORGANIZATION U.S. Army Aeromedical Research Laboratory 6b. OFFICE SYMBOL (If applicable) SGRD-UAD-IV	7a. NAME OF MONITORING ORGANIZATION U.S. Army Medical Research, Development, Acquisitions and Logistics Command (Provisional
6c. ADDRESS (City, State, and ZIP Code) P.O. Box 620577 Fort Rucker, AL 36362-0577	7b. ADDRESS (City, State, and ZIP Code) Fort Detrick Frederick, MD 21702-5012
8a. NAME OF FUNDING/SPONSORING ORGANIZATION 8b. OFFICE SYMBOL (If applicable)	9. PROCUREMENT INSTRUMENT IDENTIFICATION NUMBER
8c. ADDRESS (City, State, and ZIP Code)	10. SOURCE OF FUNDING NUMBERS PROGRAM ELEMENT NO. 62787A 3 PROJECT NO. 0162787A878 TASK NO. ED WORK UNIT ACCESSION NO. 141

11. TITLE (Include Security Classification)
A correlative investigation of simulated occupant motion and accident report in a helicopter crash

12. PERSONAL AUTHOR(S)
David G. Beale, Nabih M. Alem, and Barclay P. Butler

13a. TYPE OF REPORT	13b. TIME COVERED	14. DATE OF REPORT (Year, Month, Day)	15. PAGE COUNT
Final	FROM _____ TO _____	1994 August	20

16. SUPPLEMENTARY NOTATION

17. COSATI CODES			18. SUBJECT TERMS (Continue on reverse if necessary and identify by block number)
FIELD	GROUP	SUB-GROUP	motion, cockpit interior, accident investigation, impact, mathematical models
13	12		
20	11		

19. ABSTRACT (Continue on reverse if necessary and identify by block number)

The motion and contact of helicopter pilot with the cockpit interior structure during a crash are explored in this report. The study relies on accident investigation reports to estimate the helicopter kinematics at impact, then uses mathematical models (i.e., the Articulated Total Body (ATB) model) to simulate the stroking of the crashworthy seat, the action of the inertia reel and restraint system, the pilot's motion and his contact with the instrument panel. The report describes simulations of several scenarios which were conducted in order to explain the occurrence of basal skull fractures. The results confirm the injury causing scenario proposed by the accident investigation and refuted another suggested scenario. The report concludes by pointing out that biodynamic models such as the ATB can be effective tools to explore the role of inertia reels, energy-absorbing seats, inflatable airbags, and other safety devices in reducing injury to the pilot.

20. DISTRIBUTION/AVAILABILITY OF ABSTRACT	21. ABSTRACT SECURITY CLASSIFICATION
☒ UNCLASSIFIED/UNLIMITED ☐ SAME AS RPT. ☐ DTIC USERS	Unclassified
22a. NAME OF RESPONSIBLE INDIVIDUAL Chief, Science Support Center	22b. TELEPHONE (Include Area Code) 205-255-6907 22c. OFFICE SYMBOL SGRD-UAX-SI

Table of contents

List of figures

List of figures (Continued)

Introduction

In 1987, an Army Apache helicopter crashed during a training mission at Fort Rucker, Alabama, resulting in fatal injuries to the rear seat pilot and survivable injuries to the front seat copilot. Figure 1 shows the seating configuration of the two pilots. U.S. Army Safety Center (USASC) investigators at Fort Rucker, Alabama, reported the aircraft damage assessment and aircrew member injuries. U.S. Army Aeromedical Research Laboratory (USAARL) researchers at Fort Rucker, Alabama, concurrently examined the helmets, restraint systems, and crashworthy seats. Crash kinematics were derived from the investigation; including estimates of the motion of the harnessed occupants during the crash.

Summary of the accident investigation

While hovering at approximately 200 feet above ground level, a flight system component failed. Corrective actions by the pilot produced a near vertical flight path, impacting on relatively hard, dry soil in an estimated 5-degree nose down attitude, an estimated 5 degrees of roll toward the left side. The terrain sloped downward and forward about 5 degrees. The aircraft left ground scars that indicated a displacement down the slope of 5 feet from the initial impact location, with a forward displacement component of 1 foot. The aircraft landed nearly flat and remained upright on the nearly horizontal surface. These measures indicated the descent was primarily vertical. We determined the motion of the occupants during the crash could be simulated by a computer model given the simplicity of the crash kinematics.

The AH-64 Apache airframe is designed with three energy-absorbing components (deformable tires, collapsible landing gear, and crushable fuselage underbelly) that are intended to dissipate and lessen impact forces before they reach the helicopter floor. Ground deformation and fuselage fracture are two factors that contribute significantly to energy dissipation. From measurements of the distortion in energy-dissipating components and from experimental data of helicopter crash tests, investigators estimated the energy absorbed. The peak vertical, forward, and lateral accelerations were 41 Gz, 5 Gx and 2 Gy at the floor below the front seat with a helicopter initial vertical velocity at impact of 50 feet/second. On impact, the helicopter developed a near vertical fracture between the front and rear seat compartments. The rear portion, which contains the bulk of the helicopter mass, was lowered by about 8 inches relative to the front. The rear of the helicopter had 8 more inches of travel than the front, reducing the vertical Gs transmitted to the floor of the rear seat. Since the front seat pilot survived and the rear did not, despite less acceleration forces, USAARL investigators searched for other less obvious causes of death. Our attention eventually focused on the helmet, the glare shield, and the retractor of the shoulder straps of the harness. Unfortunately, the fracture caused the glare shield of the rear seat instrument panel to be pushed up 8 inches from its normal position in the cabin, and into the strike envelope of the helmeted rear seated pilot, as diagrammed in Figure 2.

The copilot had a burst fracture to L3 lumbar vertebrae. This fracture is a major injury, but survivable. Because he sustained only minor head injuries despite the presence of the optical relay tube sighting equipment very close to his head, the automatic retractor was assumed to have locked, preventing any significant reeling of the shoulder belt.

The autopsy report of the rear seat pilot indicated death was a result of a basilar skull fracture. Approximately 12 inches of harness belt were spooled out, calling into question whether the inertia reel retractor, designed to lock at 3 G of belt acceleration, had functioned as intended. The pilot sustained no spinal injuries, providing further evidence that he was subject to less acceleration forces than the copilot.

An examination of the pilot's helmet revealed a set of scratches parallel to the helmet visor release knob, and evidence of an impact to the helmet near the limit of the knob range of motion. The knob was left at its uppermost position on the slide track (see Figure 3). This led to the hypothesis that the pilot's helmet impacted and became wedged under the glare shield, as displayed in Figure 2. Further forward motion of the neck and body, while the head essentially remained motionless under the glare shield, transmitted a force system of magnitude, direction, and duration large enough to produce the basilar skull fracture. In our study, we test this hypothesis by using crash simulation software, enhancing our understanding of the kinematics of interaction between the pilot and cockpit during a helicopter mishap.

The biodynamic simulation

Occupant biodynamics were reconstructed using the DYNAMAN program (GESAC, Inc., 1992), a software package which is based on the articulated total body (ATB) computational simulation software (Fleck, Butler, and Vogel, 1975; Obergefell et al. 1988). Given as input a number of body segments connected by mathematical representations of common joints, the ATB automatically formulates the ordinary differential equations that govern the body motion. For a given set of initial positions and velocities of these segments, ATB integrated those equations and provided time-histories of the kinematics which then are post-processed to generate graphical representations of motion. The software produced time histories of plots of forces, displacements, velocities, and accelerations of body segments which are used to predict injuries. Head and neck injury criteria were used to predict pilot injuries, and the dynamic response index (DRI) applied to predict spinal injuries to the copilot. The predictions were compared to actual injuries received by the two occupants. Results of the ATB simulations were used to draw conclusions about occupant motion and possible injury mechanisms and assess the safety equipment performance.

Modelling

The initial impact velocity and the time history of the accelerations of the helicopter cabin floor are necessary input to the software. These data are derived from the site investigation of the damaged aircraft, followed by an analysis based on the work energy theorem to account for energy

losses during the crash and simple kinematic equations for rectilinear motion of a mass. The landing can be likened to collapsing a contractible telescope or dropping a spring-mass-damper system with the larger stiffness and damping rates closer to mass and further from the point of impact (Figure 4). At the onset of the impact, tires and landing gear collapsed, followed by the crush of the fuselage underbelly against the ground, and finally a fuselage fracture. Each collapse mechanism removes vehicle energy while reducing the Gs transferred to the helicopter floor. This simple model works well for the rear seat occupant because the bulk of the helicopter mass is behind the fracture.

Experimental crash test data allow the approximation of the floor vertical acceleration as a constant during tire and landing gear collapse and as a triangular profile during fuselage crush, fracture, and soil depression (Coltman et al., 1989). Given the kinematic relations using the symbols a, v, s, for acceleration, velocity, and displacement, respectively:

$$\int dv = \int a\,dt \quad \text{and} \quad \int ds = \int v\,dt$$

Assuming constant acceleration over time from initial conditions $t_0 = 0$ sec and v_0 (as yet unknown vertical impact velocity), and where A is the acceleration in G and v_1 is a velocity (ft/sec) and less than v_0 at t_1, it can be shown (Zimmermann, and Merritt, 1989) that the end of the pulse occurs at t_1 defined by:

$$t_1 = \frac{v_0 - v_1}{32.2A} \tag{1}$$

Also, where s_Δ is the distance of collapse of the tires and landing gear (46/12 = 3.83 feet).

$$A = \frac{v_0^2 - v_1^2}{64.4 s_\Delta} \tag{2}$$

Similarly, integrating the kinematic relations for a triangular pulse between t_1 and t_2 yields:

$$t_2 - t_1 = \frac{2 v_1}{32.2 A_{max}} \tag{3}$$

and

$$s_\Delta = \frac{v_1^2}{32.2 A_{max}} \tag{4}$$

where s_Δ is taken here as 1.5 feet of soil depression, fuselage crush, and fracture, and A_{max} is the peak acceleration of the triangular pulse. Last, experimental data indicative of the energy that is

absorbed during landing (or equivalently, work performed to deform soil and helicopter and to fully collapse the landing gear) is required to complete the estimation of the acceleration profile. Assuming that landing gear alone can dissipate the kinetic energy of a 33 ft/sec vertical drop, then the work energy theorem implies:

$$v_0^2 - v_1^2 = 33^2 \qquad (5)$$

Accident investigators estimated the work or energy of the soil depression, fuselage crush, and fracture as representative of a 35.57 ft/sec velocity change. Hence, since v_2 (velocity at the end of the acceleration pulse) is 0 ft/sec, then v_1 must be 35.57 ft/sec for the rear seat. From equation 5, the initial velocity v_0 equals 48.5 ft/sec. From equation 2, the acceleration plateau A equals 4.411 G. Equation 1 gives a time t_1 of 0.091 seconds. The peak of acceleration triangle, G_{max} is 26.2 Gs from equation 4. Finally, from equation 3, end of the pulse occurs at t_2 of 0.175 seconds. The acceleration pulse time history for the back seat pilot is plotted in Figure 5.

Because of the fracture between front and rear, the triangular acceleration pulse at the front seat floor had to be shorter in duration and more severe in magnitude. Since fracture occurred after collapse of the landing gear, the acceleration plateau A, velocities v_0 and v_1, and displacement s_Δ should be the same as the front seat during the plateau portion of the pulse. The displacement during the triangular pulse was decreased to 10 inches, so s_Δ is 0.833 ft. Substituting this value of s_Δ and $v_1 = 35.57$ ft /sec into equation 4, we obtain $A_{max} = 47$ G. From equation 3, the acceleration pulse ends at $t_2 = 0.138$ seconds, and the pulse is shown in Figure 6. Both Figures 5 and 6 have been smoothed, and sloped at early time to account for a more realistic and gradual Gz acceleration onset due to tire deflection. Forward Gx acceleration was taken as a similar profile to the Gz, but proportionately reduced to reflect A_{max} of only 5 G.

Once the acceleration pulse was transmitted to the helicopter floor, further attenuation of the signal was provided by the seat cushion and the energy absorber between the seat and floor. The energy absorber provided a near constant force characteristic versus displacement once a 3540-pound force threshold was reached, as shown in Figure 7. This device would not activate until a certain G level was transmitted to the seat and pilot. For the copilot, the seat stroked between 5 and 6 inches, whereas the pilot rear seat stroked approximately 1 inch. In both instances, the floor upward displacement impeded the seats' downward motion.

The model included body segment properties which were determined by GEBOD, another component of the simulation software (Gross, 1991.) The model also included a harness belt system and retractor to lock the shoulder belts at a desired time in the simulation. In simulations of the rear seat pilot, the glare shield was placed in its final position because it was anticipated that the glare shield was in its final position relative to the occupant before helmet impact. A helmet of the correct inertia and mass as measured in a laboratory was added to the head segment, which now is referred to as the head/helmet segment.

Results of simulations

Two scenarios for the pilot's biodynamics were simulated to attempt to achieve agreement with his helmet damage, glare shield deformation, and injury evidence. A third simulation of the copilot also was performed. The three simulations are discussed as follows:

Simulation 1: Pilot's helmet impacts the glare shield during forward motion

This simulated scenario, where the visor knob impacts the glare shield during the forward motion of the pilot causing the helmet to be wedged under the shield, represents the conclusion of the original accident report. Figure 8 shows the sequence of pilot motion, with the initial seated position that corresponds to the onset of the acceleration pulse, i.e., at 0 milliseconds (ms). The graphics in this figure include the knob on the helmet, and the glare shield in its final position. At 100 ms in Figure 8, the occupant leans forward with an increase of relative angle between head and neck. In this scenario, the harness belts are locked at 140 ms in a effort to duplicate the approximate position of the locked belt in the actual mishap. Just before 144 ms, the large acceleration spike causes approximately 1 inch of deformation in the energy absorber. At 144 ms in Figure 8, the head/helmet segment just is touching the glare shield for the first time. Contact between helmet and glare shield continues as the glare shield rides up the helmet until the glare shield impacts the helmet knob at 156 ms. Immediately after impact, the knob rebounds off the glare shield in Figure 8 at 164 ms and head/helmet motion continues below the glare shield.

Between 164 and 180 ms (see Figure 8), the head goes through a rotation as the forces that have developed in stretching the harness belts pull the torso back into the seat. Eventually, the occupant would be pulled back by the harness belt to the upright seated position. Figure 9 is an overlay of the head/helmet as it moves under the glare shield. As the head contacts the glare shield, the angle between the neck and head increases, increasing the likelihood of serious injury. When the knob impacts the glare shield, the angle between the neck and head increases substantially and, most probably, the basilar skull fracture occurred immediately after the knob impacted the glare shield. Other evidence which supports this scenario includes the absence of damages to the instrument panel and helmet shell indicating an impact of some sort on the helmet at the knob.

The force components in the neck along the aircraft X and Z directions, shown in Figures 10 and 11, have a resultant neck force that exceeds 1000 pounds for the period from 160 to 165 ms, a magnitude and duration sufficient to cause serious neck injury (Coltman et al., 1989.) The simulation results are susceptible to stiffness and friction coefficient of the glare shield and helmet, and the position of the glare shield itself. These are all parameters which only can be estimated or known within a relatively large range. Adjusting these parameters could produce simulations with larger neck forces, but will still demonstrate the same qualitative response as this simulation.

Finally, the potential that inertia reels failed to lock at 3 G, as designed, was explored. A recent USAARL study tested 110 inertia reels in the field at Fort Rucker and found 24.5 percent failed to lock at the 3 G requirement (McEntire, 1992.) This suspected failure in the Apache mishap was supported further by evidence of approximately 12 inches of nonspooled shoulder belt from

the pilot's inertia reel. Figure 12a shows a time history plot of the Gx acceleration of the upper torso relative to the seat back, which is equivalent approximately to acceleration of the belt as it unspools. The plot shows acceleration did not exceed the locking threshold until approximately 130 ms. The locking of the belt was simulated to occur at 150 ms. Note that at about 70 ms, the Gx may have been as high as 4 G; however, the Gz at that time was about 12, indicating the torso was moving down into the seat and tended to relax the belt despite the forward acceleration trend.

Although the ATB formulation used in these simulations was not designed to generate the linear acceleration of the belt at it spools out of the inertia reel, the generated output was manipulated to extract shoulder harness extension versus time. The output was numerically differentiated to produce harness belt acceleration at 1 ms intervals. Next, the accelerations were smoothed by a running average over 5 points (5-ms window), and plotted in Figure 12b. The computed belt acceleration (Figure 12b) indicates the 3-G level was exceeded at 70 ms into the simulation for about 10 ms. Beyond 120 ms, an acceleration pulse occurred and, most likely, activated the inertia reel locking mechanism. The large acceleration at 150 ms occurred as the harness locked normally in response to the crash forces. The plot also indicates the simulated belt acceleration may have reached or exceeded the 3 G locking threshold at an earlier time (70 ms) than had occurred in the actual accident. Keep in mind the inertia reel locking mechanism was designed to trigger at the onset of a 3 G belt acceleration. Nevertheless, uncertainties in the estimated input parameters make the results of the simulations just as uncertain. Thus, it appears there is no conclusive demonstration that the seat belt should have locked any earlier than the simulated 150 ms into the onset of the crash. Several simulations were run in which the inertia reel was permanently locked. As expected, these runs demonstrated the torso was restrained from excessive forward movement, thereby preventing injurious head/helmet contact with the glare shield.

Simulation 2: Pilot's helmet impacts glare shield on rebound

In this simulation, the only parameter adjusted was the position of the glare shield, which was moved slightly from its position in scenario 1. Figure 13 shows the pilot's head/ helmet skimming past the glare shield without significant force between glare shield and helmet. The knob impact and helmet deformation on its forward pass by the glare shield were, therefore, relatively unimportant, and so the knob was ignored here. The shoulder harness belt was locked at 140 ms and, as the belt compressed the upper torso it pulled the pilot back and his head/helmet impacted the glare shield during the rebound pass with a very large force and at the location of the impact damage on the actual helmet. Because this simulation did not generate sufficient downward forces which are generally associated with basilar skull fractures, this scenario likely did not occur.

Simulation 3: Copilot's biodynamics of motion

In the actual accident, the front seat copilot sustained a serious lumbar L3 burst fracture due to the large vertical acceleration. The investigators concluded the harness belts immediately locked. Since the seat energy absorber stroked about 6 inches in the accident, a very stiff spring that

activated for deflections beyond 5 inches was included in the simulation to limit the seat and energy absorber motion. The results of the simulation given in Figure 14 primarily show head neck motion, although relatively large forces were transmitted to the spine from the seat.

To correlate actual spinal injury of the copilot with the simulated, plots of simulated energy absorber stroke and seat vertical acceleration (Gz) are given in Figures 15 and 16, respectively. The seat stroked approximately 6 inches between 110 and 140 ms before the floor came up and limited the seat travel. During this period, the seat acceleration in Figure 16 was limited to a tolerable level of approximately 15 G. However, upon floor/seat impact, the acceleration level abruptly increased beyond 40 G. The acceleration remained above 40 G for 8 ms between 144 and 152 ms. It is accepted generally (Coltman et al., 1989; Coltman, 1986) that sustained accelerations beyond 20 G are very likely to cause spinal injury. An accepted measure of the potential to cause spinal injury is the dynamic response index (Brinkley, 1985) which was developed from experimental studies of pilots in ejection seats, and is based on the following spring-mass equation model approximation (Brinkley and Shaffer, 1971):

$$\frac{d^2\delta}{dt^2} + 25.39\frac{d\delta}{dt} + 2798\delta = 386.1A_{z,seat} \qquad (6)$$

where $A_{z,seat}$ is seat acceleration in in/sec^2. This equation must be integrated numerically because of the tabular form of the right hand side. The DRI is calculated at each time step as:

$$DRI = 7.248\delta_{max} \qquad (7)$$

where δ_{max} is the maximum value of δ as obtained from integration of equation 6. This resulted in a DRI equal to 23. This led to an estimate of probability of spinal injury rate of slightly greater than 50 percent (Brinkley, 1985). It might have been expected that this would have been larger because of the seriousness of the copilot's injury. However, this result does indicate that injury would be anticipated in this environment.

Several other simulations were performed where the seat stiff spring was removed, allowing the energy absorber to fully stroke without impacting the floor. By allowing the energy absorber to stroke a full 10 inches, it limits the acceleration to the tolerable 15-G design point. Severe injury may not have occurred. It is reasonable to conclude that the interference between the seat stroking and the usual floor motion was a significant factor in increasing the risk of spinal injury.

Conclusions

Biodynamic modeling confirmed the injury causing scenario proposed by an accident investigation team, and refuted another suggested scenario. This type of simulation is a quick and powerful tool that allows investigators to obtain reasonable estimates of the internal forces in the neck and the lower spine which cannot be obtained by other means. The ability to simulate different scenarios allowed us to conclude the stroking of front seat is all but lost in high impact accelerations when the floor buckles upwards. Used with accident evidence, we can explore how safety devices, e.g., inertia reels and energy-absorbing seats, functioned in a crash. We can increase confidence in this modeling by continuous validations of the input parameters and its acceptance and usage by enhancement of its operation.

References

Brinkley, J. W. 1985. Acceleration exposure limits for escape system advanced development. SAFE journal, volume 15, No. 2, pp. 10-16.

Brinkley, J. W., and Shaffer, J. T. 1971. Dynamic simulation techniques for the design of escape systems: Current applications and future Air Force requirements. Wright-Patterson Air Force Base, Ohio: Aerospace Medical Research Lab. AMRL Technical Report 71-292.

Coltman, J. W. 1986. Crash-resistant crewseat limit-load optimization through dynamic testing with cadavers. Simula Inc., Fort Eustis, Virginia: Aviation Applied Technology Directorate, U.S. Army Aviation Research and Technology Activity, USAAVSCOM TR-85-D-11.

Coltman, J. W., Van Ingen, C., Johnson, N. B., and Zimmermann, R. E. 1989. Aircraft crash survival design guide. volume II: Aircraft design crash impact conditions and human tolerance. Fort Eustis, VA: Aviation Applied Technology Directorate. USAAVSCOM TR 89-D-22B.

Fleck, J. T., Butler, F. E., and Vogel, S. L. 1975. An improved three-dimensional computer simulation of crash victims. NHTSA reports. DOT-HS-801-507 through 510.

GESAC, Inc. 1992. DYNFEM user's manual. Kearneysville, WV: GESAC, Inc.

Gross, M. E. 1991. The GEBOD III program user's guide and description. Air Force Report AL-TR-1991-0102.

McEntire, B. Joseph. 1992. U.S. Army helicopter inertia reel locking failures. Paper presented at the annual symposium of the Advisory Group for Aerospace Research and Development (AGARD), April in Cesme, Turkey.

Obergefell, Louise A., Fleck, John T., Kaleps, Ints, and Gardner, Thomas R. 1988. Articulated total body model enhancements: volume 1: Modifications. Wright-Patterson Air Force Base, OH: Harry G. Armstrong Aerospace Medical Research Laboratory. AAMRL-TR-88-009.

Zimmermann, R. E., and Merritt, N. A. 1989. Aircraft crash survival design guide. Volume I: Design criteria and checklists. Fort Eustis, VA: Aviation Applied Technology Directorate. USAAVSCOM TR 89-D-22A.

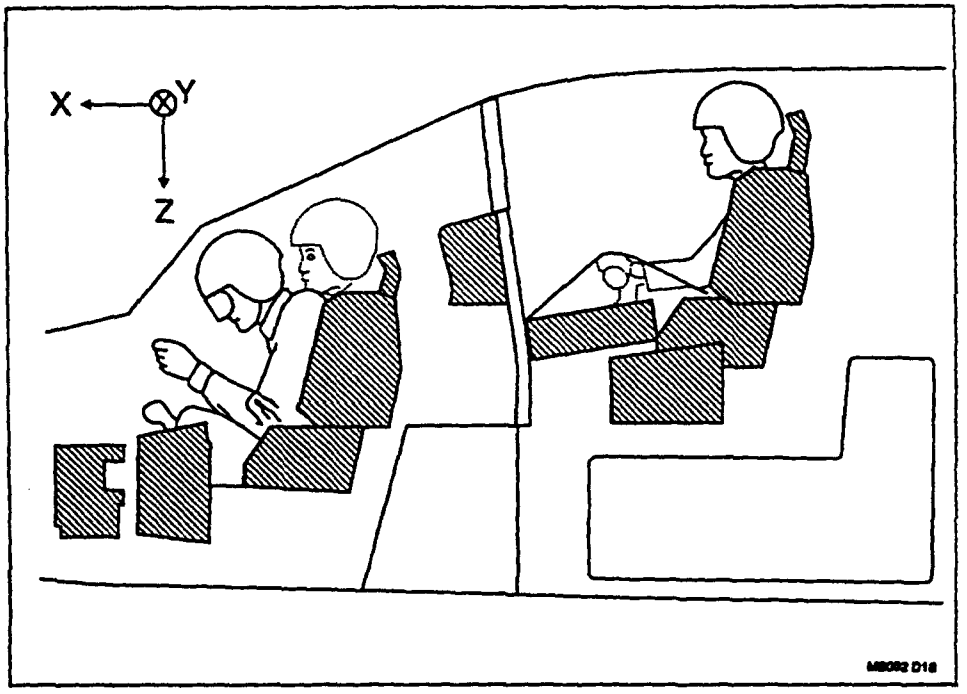

Figure 1. Front and rear seat occupant positions in Apache helicopter.

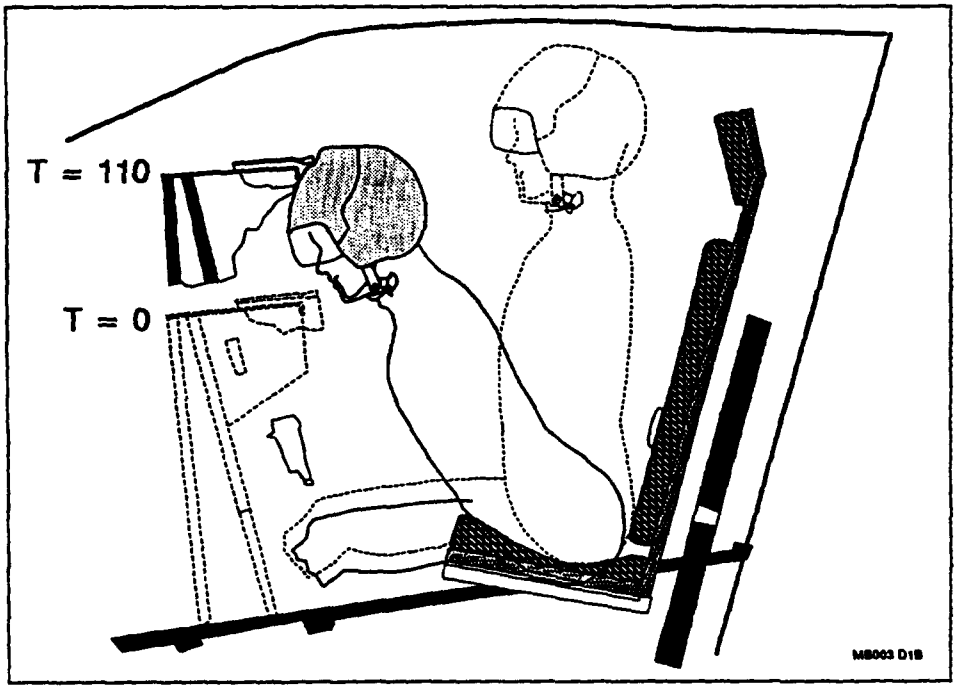

Figure 2. Rear seat occupant motion as conjectured from accident investigation.

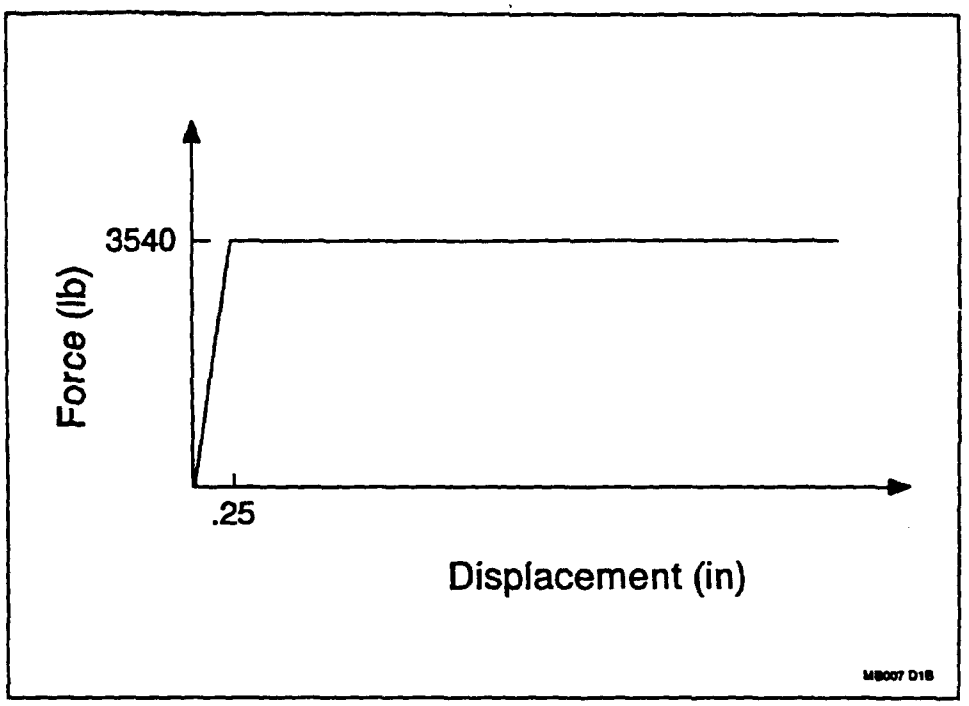

Figure 3. Helmet profile.

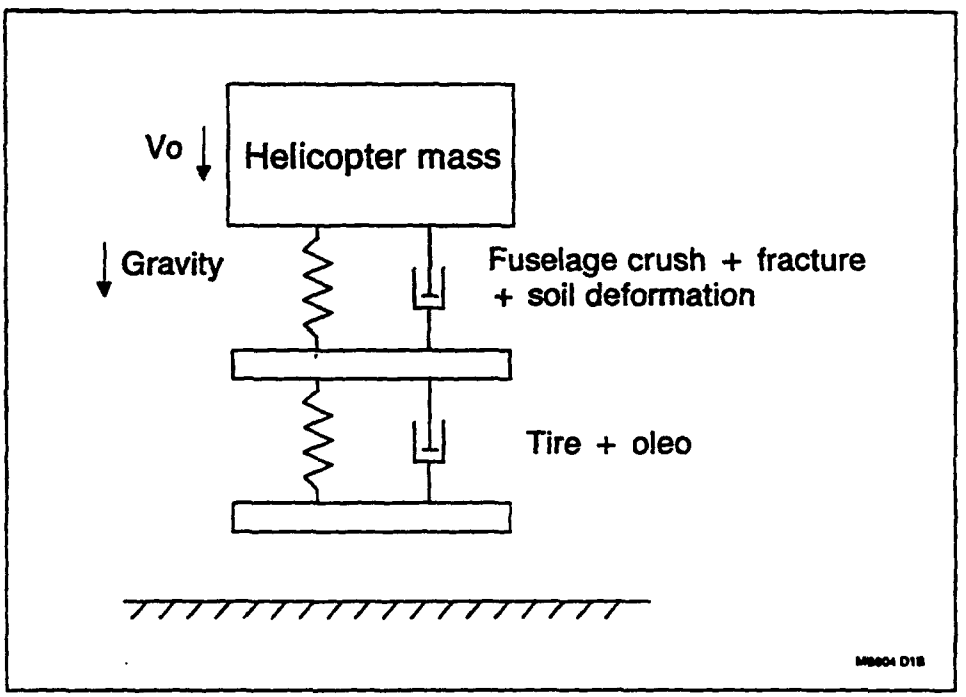

Figure 4. Spring-damper-mass idealization of crashing helicopter in a vertical descent.

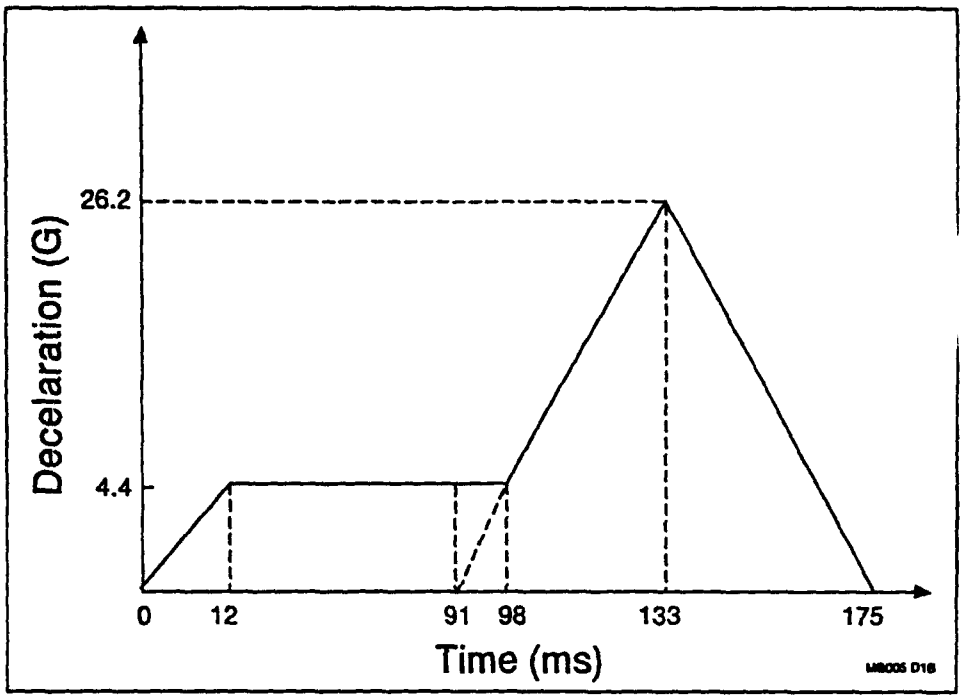

Figure 5. Vertical (Z) acceleration vs. time for floor of rear seat.

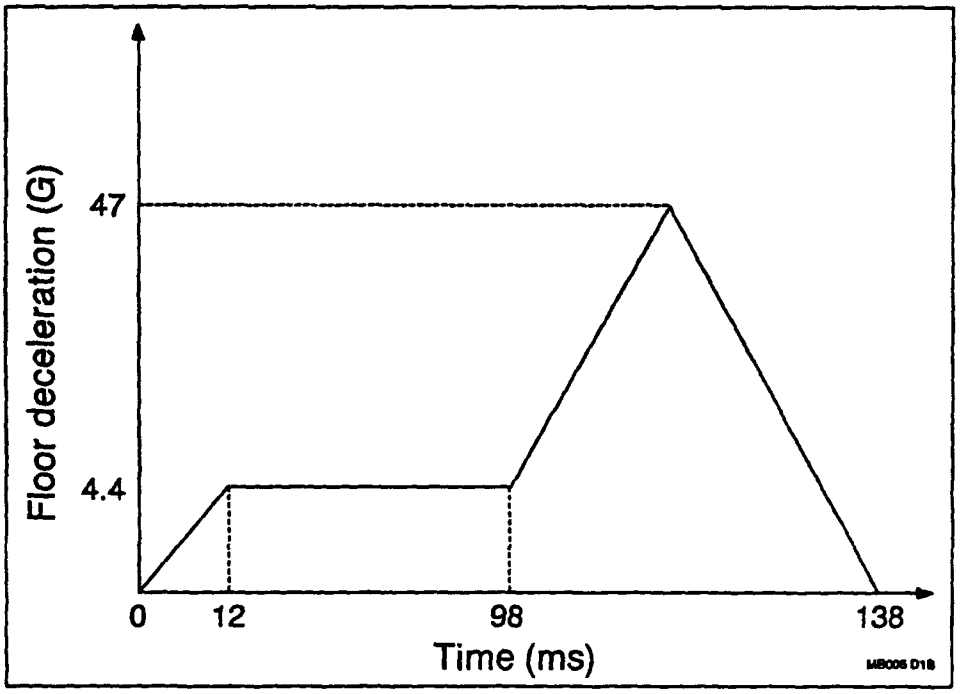

Figure 6. Vertical (Z) acceleration vs. time for floor of front seat.

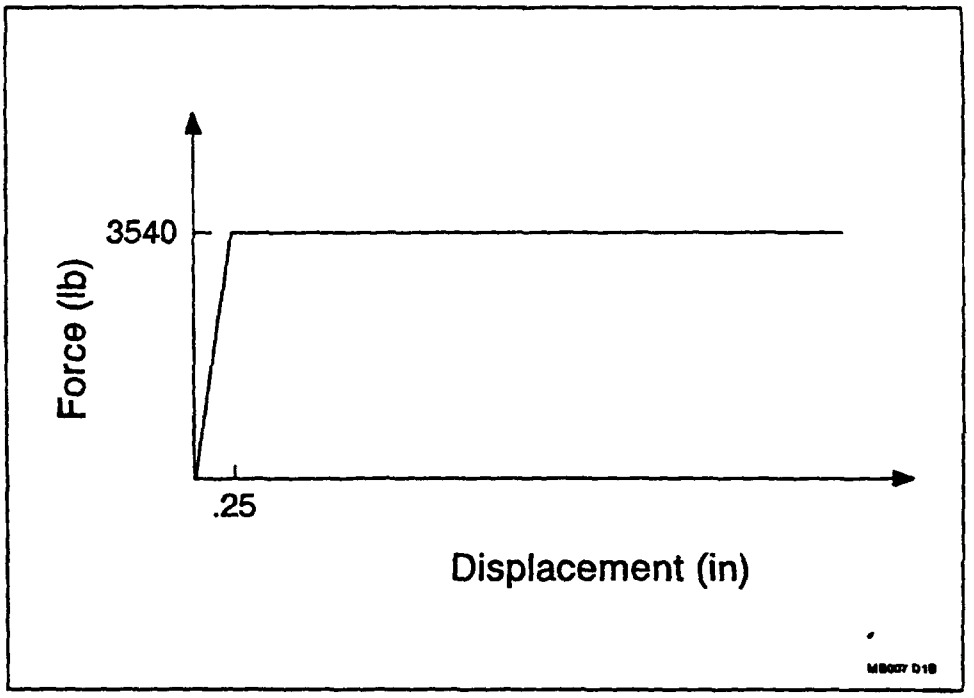

Figure 7. Seat energy absorber force-displacement characteristic.

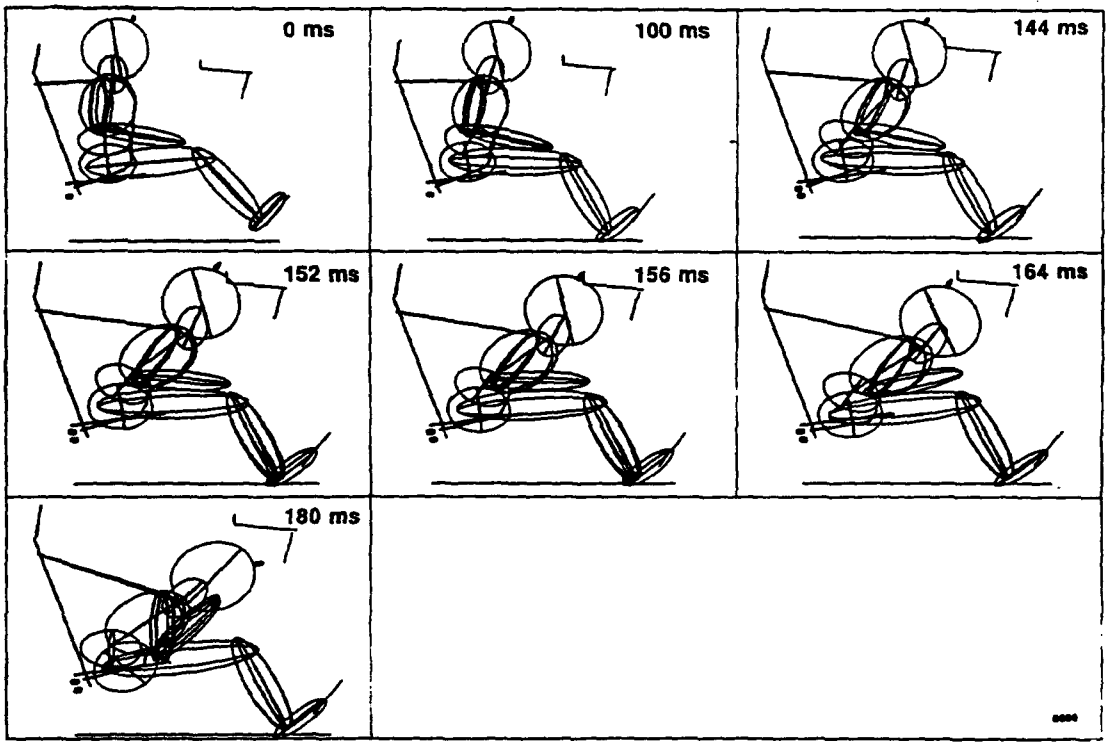

Figure 8. Graphics of 180 ms of whole body motion for scenario 1 simulation.

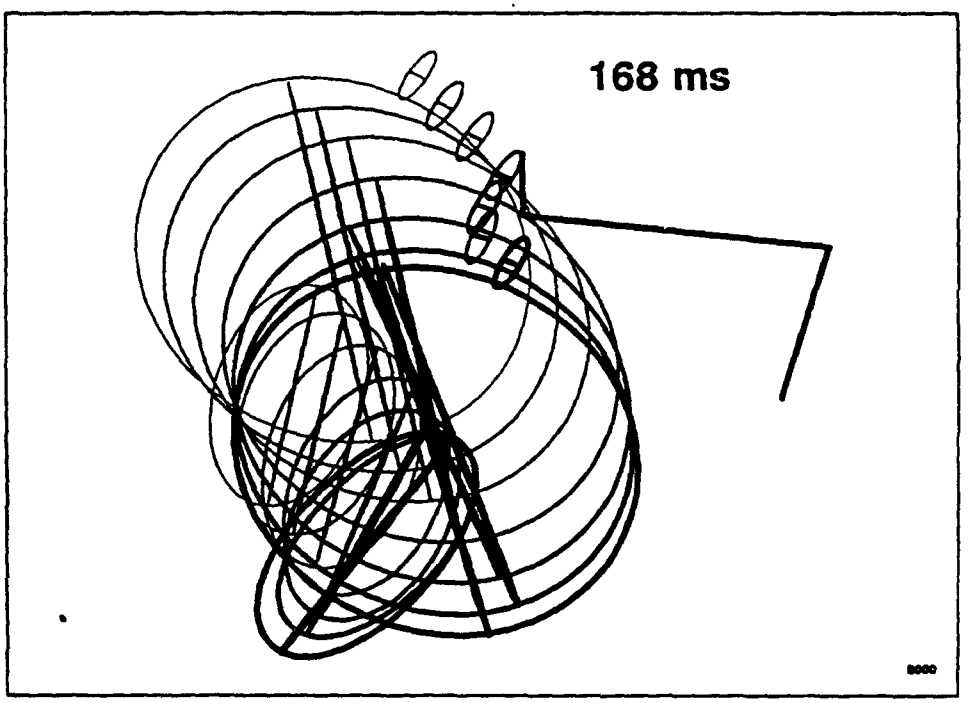

Figure 9. Graphics of head and neck motion through glare shield impact for simulation of scenario 1.

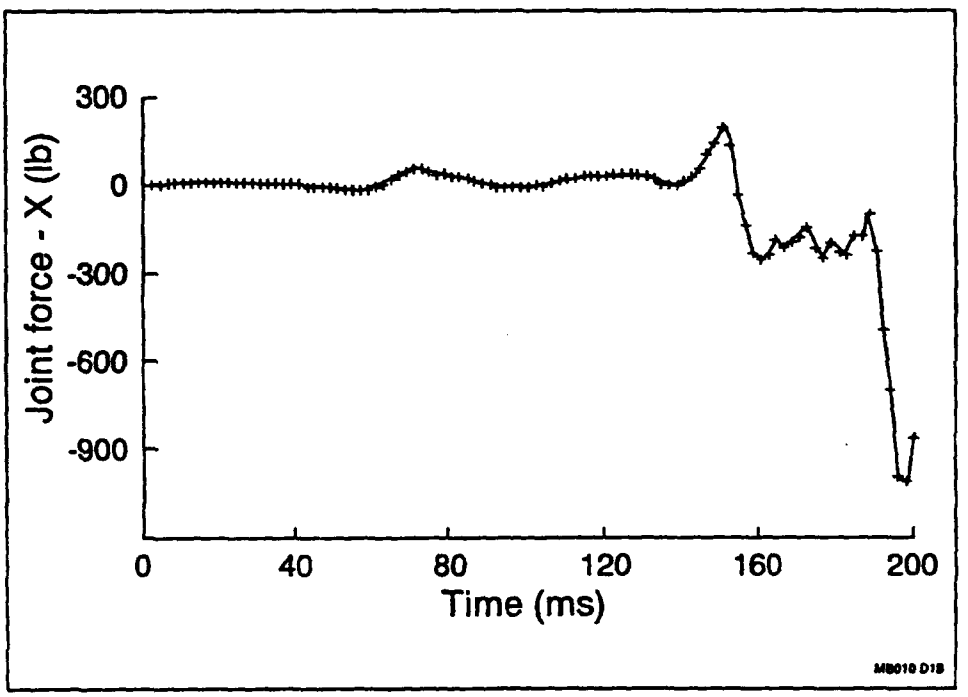

Figure 10. Forward (X) component of force in neck vs. time for simulation 1.

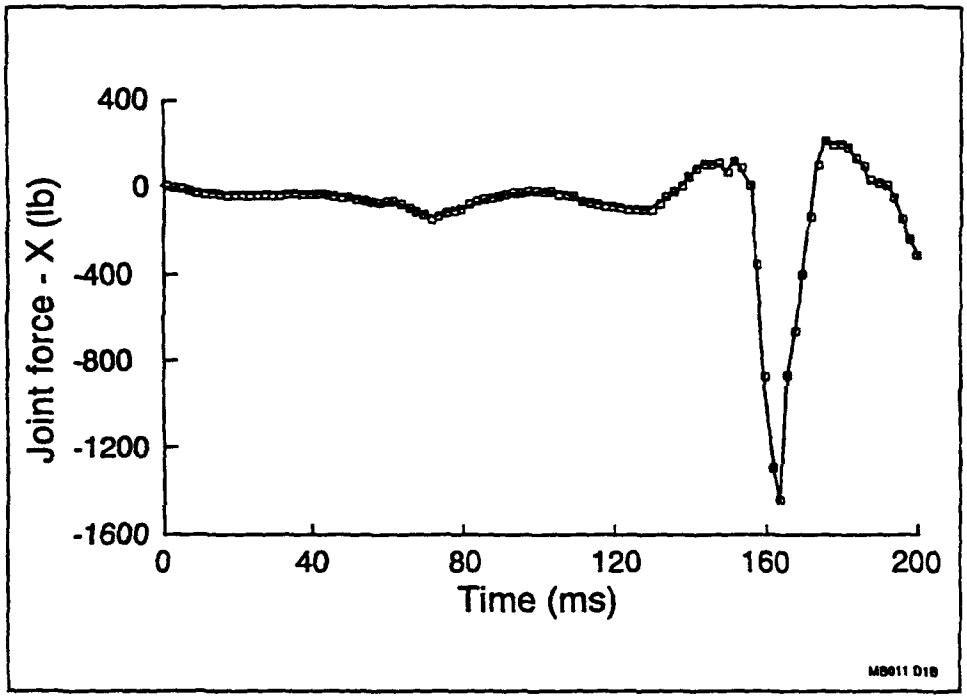

Figure 11. Vertical (Z) component of force in neck vs. time for simulation 1.

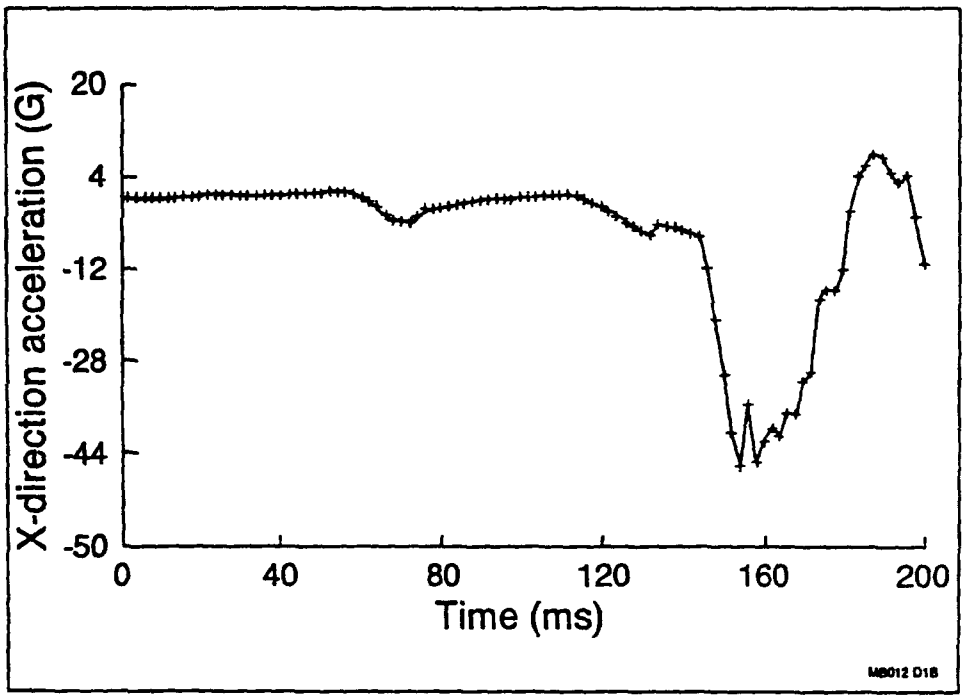

Figure 12a. Forward (X) component of upper torso acceleration vs. time for simulation 1.

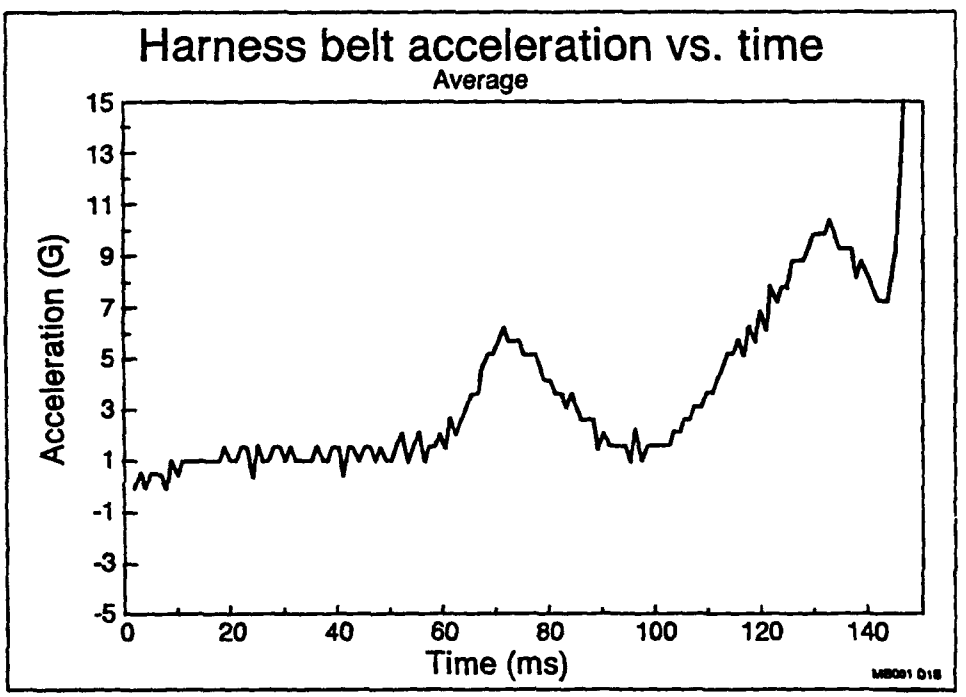

Figure 12b. Harness belt acceleration obtained by double differentiation of output of simulation 1.

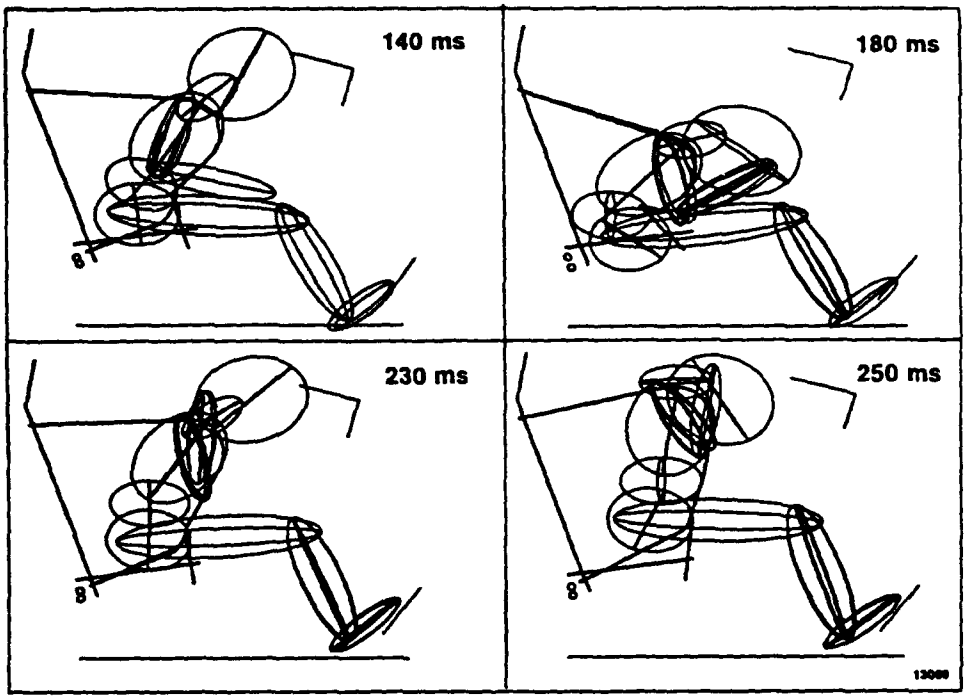

Figure 13. Graphics of whole body motion through glare shield impact for simulation 2.

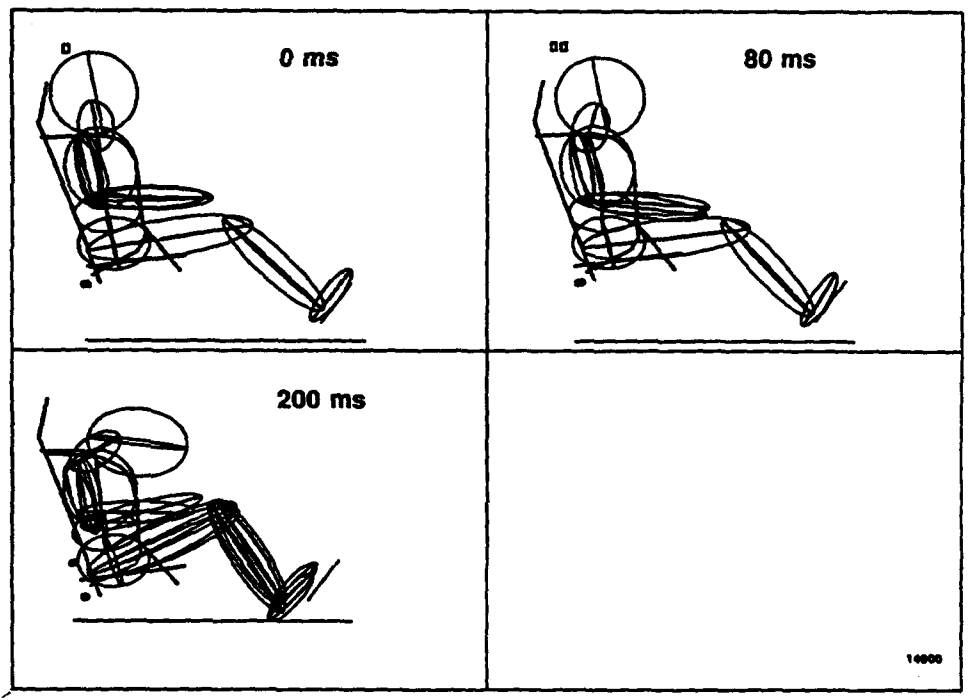

Figure 14. Graphics of 200 ms of whole-body motion for simulation 3.

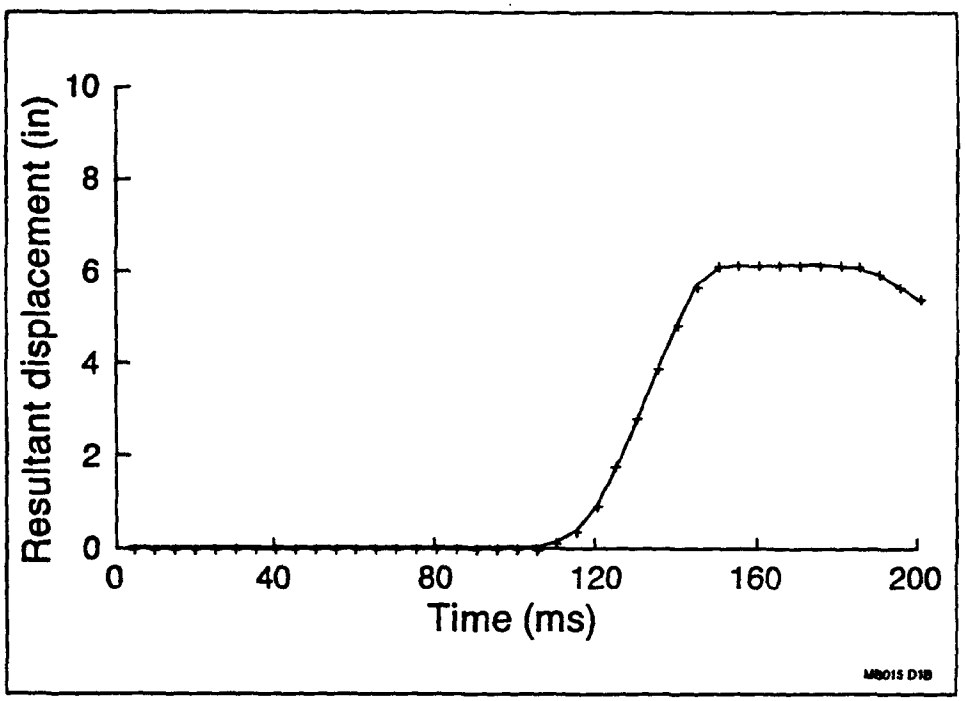

Figure 15. Vertical stroke vs. time for front seat in simulation 3.

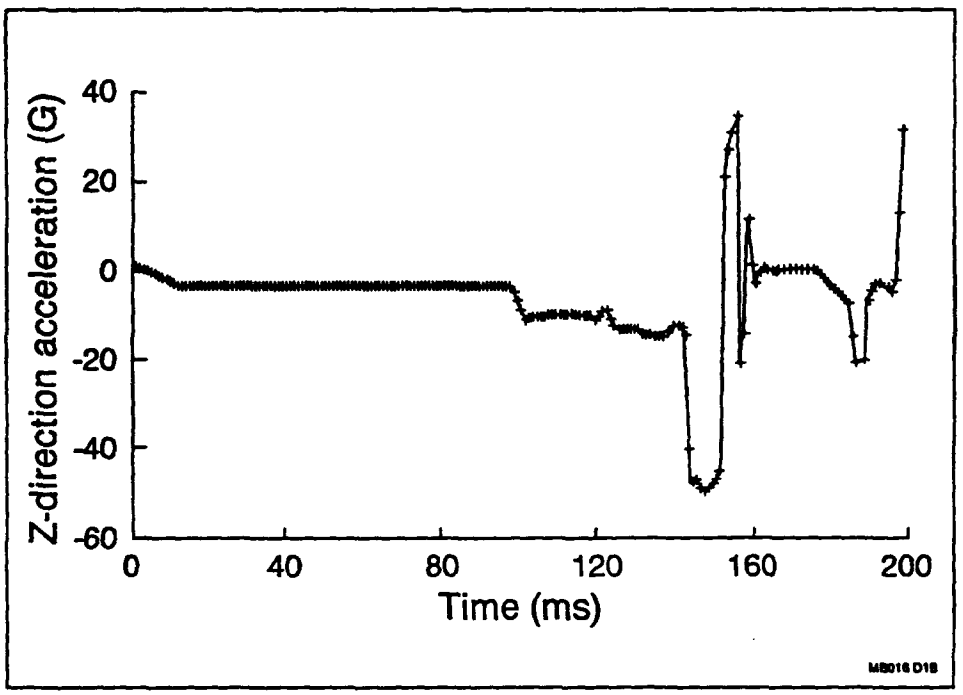

Figure 16. Vertical acceleration vs. time for front seat in simulation 3.

Initial distribution

Commander, U.S. Army Natick Research, Development and Engineering Center
ATTN: SATNC-MIL (Documents Librarian)
Natick, MA 01760-5040

Chairman
National Transportation Safety Board
800 Independence Avenue, S.W.
Washington, DC 20594

Commander
10th Medical Laboratory
ATTN: Audiologist
APO New York 09180

Naval Air Development Center
Technical Information Division
Technical Support Detachment
Warminster, PA 18974

Commanding Officer, Naval Medical Research and Development Command
National Naval Medical Center
Bethesda, MD 20814-5044

Deputy Director, Defense Research and Engineering
ATTN: Military Assistant for Medical and Life Sciences
Washington, DC 20301-3080

Commander, U.S. Army Research Institute of Environmental Medicine
Natick, MA 01760

Library
Naval Submarine Medical Research Lab
Box 900, Naval Sub Base
Groton, CT 06349-5900

Executive Director, U.S. Army Human Research and Engineering Directorate
ATTN: Technical Library
Aberdeen Proving Ground, MD 21005

Commander
Man-Machine Integration System
Code 602
Naval Air Development Center
Warminster, PA 18974

Commander
Naval Air Development Center
ATTN: Code 602-B
Warminster, PA 18974

Commanding Officer
Armstrong Laboratory
Wright-Patterson
Air Force Base, OH 45433-6573

Director
Army Audiology and Speech Center
Walter Reed Army Medical Center
Washington, DC 20307-5001

Commander/Director
U.S. Army Combat Surveillance and Target Acquisition Lab
ATTN: SFAE-IEW-JS
Fort Monmouth, NJ 07703-5305

Director
Federal Aviation Administration
FAA Technical Center
Atlantic City, NJ 08405

Director
Walter Reed Army Institute of Research
Washington, DC 20307-5100

Commander, U.S. Army Test
and Evaluation Command
Directorate for Test and Evaluation
ATTN: AMSTE-TA-M (Human Factors
Group)
Aberdeen Proving Ground,
MD 21005-5055

Naval Air Systems Command
Technical Air Library 950D
Room 278, Jefferson Plaza II
Department of the Navy
Washington, DC 20361

Director
U.S. Army Ballistic
Research Laboratory
ATTN: DRXBR-OD-ST Tech Reports
Aberdeen Proving Ground, MD 21005

Commander
U.S. Army Medical Research
Institute of Chemical Defense
ATTN: SGRD-UV-AO
Aberdeen Proving Ground,
MD 21010-5425

Commander
USAMRMC
ATTN: SGRD-RMS
Fort Detrick, Frederick, MD 21702-5012

HQ DA (DASG-PSP-O)
5109 Leesburg Pike
Falls Church, VA 22041-3258

Harry Diamond Laboratories
ATTN: Technical Information Branch
2800 Powder Mill Road
Adelphi, MD 20783-1197

U.S. Army Materiel Systems
Analysis Agency
ATTN: AMXSY-PA (Reports Processing)
Aberdeen Proving Ground
MD 21005-5071

U.S. Army Ordnance Center
and School Library
Simpson Hall, Building 3071
Aberdeen Proving Ground, MD 21005

U.S. Army Environmental
Hygiene Agency
ATTN: HSHB-MO-A
Aberdeen Proving Ground, MD 21010

Technical Library Chemical Research
and Development Center
Aberdeen Proving Ground, MD
21010-5423

Commander
U.S. Army Medical Research
Institute of Infectious Disease
ATTN: SGRD-UIZ-C
Fort Detrick, Frederick, MD 21702

Director, Biological
Sciences Division
Office of Naval Research
600 North Quincy Street
Arlington, VA 22217

Commandant
U.S. Army Aviation
Logistics School ATTN: ATSQ-TDN
Fort Eustis, VA 23604

Headquarters (ATMD)
U.S. Army Training
and Doctrine Command
ATTN: ATBO-M
Fort Monroe, VA 23651

IAF Liaison Officer for Safety
USAF Safety Agency/SEFF
9750 Avenue G, SE
Kirtland Air Force Base
NM 87117-5671

Naval Aerospace Medical
Institute Library
Building 1953, Code 03L
Pensacola, FL 32508-5600

Command Surgeon
HQ USCENTCOM (CCSG)
U.S. Central Command
MacDill Air Force Base, FL 33608

Director
Directorate of Combat Developments
ATTN: ATZQ-CD
Building 515
Fort Rucker, AL 36362

U.S. Air Force Institute
of Technology (AFIT/LDEE)
Building 640, Area B
Wright-Patterson
Air Force Base, OH 45433

Henry L. Taylor
Director, Institute of Aviation
University of Illinois-Willard Airport
Savoy, IL 61874

Chief, National Guard Bureau
ATTN: NGB-ARS
Arlington Hall Station
111 South George Mason Drive
Arlington, VA 22204-1382

AAMRL/HEX
Wright-Patterson
Air Force Base, OH 45433

Commander
U.S. Army Aviation and Troop Command
ATTN: AMSAT-R-ES
4300 Goodfellow Bouvelard
St. Louis, MO 63120-1798

U.S. Army Aviation and Troop Command
Library and Information Center Branch
ATTN: AMSAV-DIL
4300 Goodfellow Boulevard
St. Louis, MO 63120

Federal Aviation Administration
Civil Aeromedical Institute
Library AAM-400A
P.O. Box 25082
Oklahoma City, OK 73125

Commander
U.S. Army Medical Department
and School
ATTN: Library
Fort Sam Houston, TX 78234

Commander
U.S. Army Institute of Surgical Research
ATTN: SGRD-USM
Fort Sam Houston, TX 78234-6200

Air University Library
(AUL/LSE)
Maxwell Air Force Base, AL 36112

Product Manager
Aviation Life Support Equipment
ATTN: SFAE-AV-LSE
4300 Goodfellow Boulevard
St. Louis, MO 63120-1798

Commander and Director
USAE Waterways Experiment Station
ATTN: CEWES-IM-MI-R,
CD Department
3909 Halls Ferry Road
Vicksburg, MS 39180-6199

Commanding Officer
Naval Biodynamics Laboratory
P.O. Box 24907
New Orleans, LA 70189-0407

Assistant Commandant
U.S. Army Field Artillery School
ATTN: Morris Swott Technical Library
Fort Sill, OK 73503-0312

Mr. Peter Seib
Human Engineering Crew Station
Box 266
Westland Helicopters Limited
Yeovil, Somerset BA20 2YB UK

U.S. Army Dugway Proving Ground
Technical Library, Building 5330
Dugway, UT 84022

U.S. Army Yuma Proving Ground
Technical Library
Yuma, AZ 85364

AFFTC Technical Library
6510 TW/TSTL
Edwards Air Force Base,
CA 93523-5000

Commander
Code 3431
Naval Weapons Center
China Lake, CA 93555

Aeromechanics Laboratory
U.S. Army Research and Technical Labs
Ames Research Center, M/S 215-1
Moffett Field, CA 94035

Sixth U.S. Army
ATTN: SMA
Presidio of San Francisco, CA 94129

Commander
U.S. Army Aeromedical Center
Fort Rucker, AL 36362

Strughold Aeromedical Library
Document Service Section
2511 Kennedy Circle
Brooks Air Force Base, TX 78235-5122

Dr. Diane Damos
Department of Human Factors
ISSM, USC
Los Angeles, CA 90089-0021

U.S. Army White Sands
Missile Range
ATTN: STEWS-IM-ST
White Sands Missile Range, NM 88002

U.S. Army Aviation Engineering
Flight Activity
ATTN: SAVTE-M (Tech Lib) Stop 217
Edwards Air Force Base, CA 93523-5000

Ms. Sandra G. Hart
Ames Research Center
MS 262-3
Moffett Field, CA 94035

Commander
USAMRMC
ATTN: SGRD-UMZ
Fort Detrick, Frederick, MD 21702-5009

Commander
U.S. Army Health Services Command
ATTN: HSOP-SO
Fort Sam Houston, TX 78234-6000

U. S. Army Research Institute
Aviation R&D Activity
ATTN: PERI-IR
Fort Rucker, AL 36362

Commander
U.S. Army Safety Center
Fort Rucker, AL 36362

U.S. Army Aircraft Development
Test Activity
ATTN: STEBG-MP-P
Cairns Army Air Field
Fort Rucker, AL 36362

Commander
USAMRMC
ATTN: SGRD-PLC (COL R. Gifford)
Fort Detrick, Frederick, MD 21702

TRADOC Aviation LO
Unit 21551, Box A-209-A
APO AE 09777

Netherlands Army Liaison Office
Building 602
Fort Rucker, AL 36362

British Army Liaison Office
Building 602
Fort Rucker, AL 36362

Italian Army Liaison Office
Building 602
Fort Rucker, AL 36362

Directorate of Training Development
Building 502
Fort Rucker, AL 36362

Chief
USAHEL/USAAVNC Field Office
P. O. Box 716
Fort Rucker, AL 36362-5349

Commander, U.S. Army Aviation Center
and Fort Rucker
ATTN: ATZQ-CG
Fort Rucker, AL 36362

Chief
Test & Evaluation Coordinating Board
Cairns Army Air Field
Fort Rucker, AL 36362

Canadian Army Liaison Office
Building 602
Fort Rucker, AL 36362

German Army Liaison Office
Building 602
Fort Rucker, AL 36362

French Army Liaison Office
USAAVNC (Building 602)
Fort Rucker, AL 36362-5021

Australian Army Liaison Office
Building 602
Fort Rucker, AL 36362

Dr. Garrison Rapmund
6 Burning Tree Court
Bethesda, MD 20817

Commandant, Royal Air Force
Institute of Aviation Medicine
Farnborough, Hampshire GU14 6SZ UK

Defense Technical Information
Cameron Station, Building 5
Alexandra, VA 22304-6145

Commander, U.S. Army Foreign Science
and Technology Center
AIFRTA (Davis)
220 7th Street, NE
Charlottesville, VA 22901-5396

Commander
Applied Technology Laboratory
USARTL-ATCOM
ATTN: Library, Building 401
Fort Eustis, VA 23604

Commander, U.S. Air Force
Development Test Center
101 West D Avenue, Suite 117
Eglin Air Force Base, FL 32542-5495

Aviation Medicine Clinic
TMC #22, SAAF
Fort Bragg, NC 28305

Dr. H. Dix Christensen
Bio-Medical Science Building, Room 753
Post Office Box 26901
Oklahoma City, OK 73190

Commander, U.S. Army Missile
Command
Redstone Scientific Information Center
ATTN: AMSMI-RD-CS-R
/ILL Documents
Redstone Arsenal, AL 35898

Aerospace Medicine Team
HQ ACC/SGST3
162 Dodd Boulevard, Suite 100
Langley Air Force Base,
VA 23665-1995

U.S. Army Research and Technology
Laboratories (AVSCOM)
Propulsion Laboratory MS 302-2
NASA Lewis Research Center
Cleveland, OH 44135

Commander
USAMRMC
ATTN: SGRD-ZC (COL John F. Glenn)
Fort Detrick, Frederick, MD 21702-5012

Dr. Eugene S. Channing
166 Baughman's Lane
Frederick, MD 21702-4083

U.S. Army Medical Department
and School
USAMRDALC Liaison
ATTN: HSMC-FR
Fort Sam Houston, TX 78234

NVESD
AMSEL-RD-NV-ASID-PST
(Attn: Trang Bui)
10221 Burbeck Road
Fort Belvior, VA 22060-5806

CA Av Med
HQ DAAC
Middle Wallop
Stockbridge, Hants S020 8DY UK

Dr. Christine Schlichting
Behavioral Sciences Department
Box 900, NAVUBASE NLON
Groton, CT 06349-5900

Commander
Aviation Applied Technology Directorate
ATTN: AMSAT-R-TV
Fort Eustis, VA 23604-5577

COL Yehezkel G. Caine, MD
Surgeon General, Israel Air Force
Aeromedical Center Library
P. O. Box 02166 I.D.F.
Israel

HQ ACC/DOHP
205 Dodd Boulevard, Suite 101
Langley Air Force Base,
VA 23665-2789

41st Rescue Squadron
41st RQS/SG
940 Range Road
Patrick Air Force Base,
FL 32925-5001

48th Rescue Squadron
48th RQS/SG
801 Dezonia Road
Holloman Air Force Base,
NM 88330-7715

HQ, AFOMA
ATTN: SGPA (Aerospace Medicine)
Bolling Air Force Base,
Washington, DC 20332-6128

ARNG Readiness Center
ATTN: NGB-AVN-OP
Arlington Hall Station
111 South George Mason Drive
Arlington, VA 22204-1382

35th Fighter Wing
35th FW/SG
PSC 1013
APO AE 09725-2055

66th Rescue Squadron
66th RQS/SG
4345 Tyndall Avenue
Nellis Air Force Base, NV 89191-6076

71st Rescue Squadron
71st RQS/SG
1139 Redstone Road
Patrick Air Force Base,
FL 32925-5000

Director
Aviation Research, Development
and Engineering Center
ATTN: AMSAT-R-Z
4300 Goodfellow Boulevard
St. Louis, MO 63120-1798

Commander
USAMRMC
ATTN: SGRD-ZB (COL C. Fred Tyner)
Fort Detrick, Frederick, MD 21702-5012

Commandant
U.S. Army Command and General Staff
College
ATTN: ATZL-SWS-L
Fort Levenworth, KS 66027-6900

ARNG Readiness Center
ATTN: NGB-AVN-OP
Arlington Hall Station
111 South George Mason Drive
Arlington, VA 22204-1382

Director
Army Personnel Research Establishment
Farnborough, Hants GU14 6SZ UK

Dr. A. Kornfield
895 Head Street
San Francisco, CA 94132-2813

ARNG Readiness Center
AATN: NGB-AVN-OP
Arlington Hall Station
111 South George Mason Drive
Arlington, VA 22204-1382

Cdr, PERSCOM
ATTN: TAPC-PLA
200 Stovall Street, Rm 3N25
Alexandria, VA 22332-0413

HQ, AFOMA
ATTN; SGPA (Aerospace Medicine)
Bolling Air Force Base,
Washington, DC 20332-6188